Georgia State University
ScholarWorks @ Georgia State University

Chemistry Faculty Publications   Department of Chemistry

Direct Determination of Multiple Ligand Interactions with the Extracellular Domain of the Calcium Sensing Receptor

Chen Zhang
Georgia State University, czhang5@gsu.edu

You Zhuo
Georgia State University, youzhuo@gmail.com

Heather A. Moniz
University of Georgia

Shuo Wang
University of Georgia

Kelley W. Moremen
University of Georgia

See next page for additional authors

Follow this and additional works at: http://scholarworks.gsu.edu/chemistry_facpub

Part of the Chemistry Commons

Recommended Citation

Authors

Chen Zhang, You Zhuo, Heather A. Moniz, Shuo Wang, Kelley W. Moremen, James H. Prestegard, Edward M. Brown, and Jenny J. Yang

Direct Determination of Multiple Ligand Interactions with the Extracellular Domain of the Calcium Sensing Receptor

Chen Zhang[1,2,†], You Zhuo[1†], Heather A. Moniz[3], Shuo Wang[3], Kelley W. Moremen[3],
James H. Prestegard[3], Edward M. Brown[4], Jenny J. Yang[1,2,§]

From the [1]Department of Chemistry, [2]Center for Diagnostics and Therapeutics, Georgia State University; [3]Department of Biochemistry and Molecular Biology and the Complex Carbohydrate Research Center, University of Georgia; [4]Department of Medicine, Division of Endocrinology, Brigham and Women's Hospital, Boston, MA

Running head: Determination of binding between CaSR ECD and its ligands

† These co-authors contributed equally to this work.
§To whom correspondence should be addressed: Jenny J. Yang, Department of Chemistry, Georgia State University, University Plaza, Atlanta, Georgia 30303 USA, Phone : 404-413-5520, Fax: 404-413-5551, email: jenny@gsu.edu

Background: The CaSR senses alterations in extracellular Ca^{2+} mainly through its extracellular domain.
Results: Interactions of ligands with the CaSR were characterized using purified ECD and biophysical techniques.
Conclusion: Ca^{2+} and L-Phe bind to both the complex and high mannose forms of the CaSR's ECDs and increase binding affinities for each other.
Significance: Our findings will provide an essential tool for future structural studies in GPCRs.

ABSTRACT

Numerous *in vivo* functional studies have indicated that the dimeric extracellular domain (ECD) of the CaSR plays a crucial role in regulating Ca^{2+} homeostasis by sensing Ca^{2+} and L-Phe. However, direct interaction of Ca^{2+} and Phe with the receptor's ECD and the resultant impact on its structure and associated conformational changes have been hampered by the large size of the ECD, its high degree of glycosylation, and the lack of biophysical methods to monitor weak interactions in solution. In the present study, we purified the glycosylated extracellular domain of CaSR (ECD) (residues 20~612), containing either complex or high mannose *N*-glycan structures depending on the host cell line employed for recombinant expression. Both glycosylated forms of the CaSR ECD were purified as dimers and exhibit similar secondary structures with ~50% α-helix, ~20% β-sheet content and a well buried Trp environment. Using various spectroscopic methods, we have shown that both protein variants bind Ca^{2+} with a K_d of 3.0~5.0 mM. The local conformational changes of the proteins induced by their interactions with Ca^{2+} were visualized by NMR with specific [15]N Phe-labeled forms of the ECD. Saturation transfer difference (STD) NMR approaches demonstrated for the first time a direct interaction between the CaSR ECD and L-Phe. We further demonstrated that L-Phe increases the binding affinity of the CaSR ECD for Ca^{2+}. Our findings provide new insights into the mechanisms by which Ca^{2+} and amino acids regulate the CaSR and may pave the way for exploration of the structural properties of CaSR and other members of family C of the GPCR superfamily.

INTRODUCTION

The Calcium-Sensing Receptor (CaSR) is a seven transmembrane protein that belongs to family C of the G protein-coupled receptor superfamily (1). The CaSR is named after its major function in regulating calcium homeostasis in the body. Its predominant expression in parathyroid and kidney cells allows this receptor to modulate parathyroid hormone (PTH) secretion

as well as renal calcium reabsorption (2-5). The CaSR is also widely expressed in other sites including the gastrointestinal system (6), the central nervous system (7), breast (8), and bone (9), among others, where it plays crucial roles in physiological and pathological functions, including cell proliferation, tissue differentiation and cancer development (10). In addition to its primary agonist, Ca^{2+}, the CaSR can also respond to various other stimuli, including other cations (11), amino acids (7,12), polyamines (13), and polypeptides (14). L-amino acids, especially aromatic amino acids (e.g. L-Phenylalanine), are thought to enhance the sensitivity of CaSR to the extracellular calcium concentration ($[Ca^{2+}]_o$) by interacting with the receptor's extracellular domain (ECD) as demonstrated in several *in vivo* studies using HEK293 cells transfected with the CaSR (12,15). Branched-chain amino acids (e.g. L-Aspartic acid, L-Lysine etc.) are less effective than aromatic amino acids (12). This could be one potential explanation for how dietary protein modulates $[Ca^{2+}]_o$ homeostasis in normal individuals as well as in patients with chronic renal failure (6,16).

Like many membrane receptors, the CaSR is heavily glycosylated with 11 highly conserved putative N-linked glycosylation sites (Asn-Xaa-Ser/Thr). These glycosylation sites are considered to be critical for the CaSR's cell surface expression (17). Membrane CaSR functions as a dimer and is comprised of the three major structural domains of the GPCR family C: an extracellular domain (ECD) that covers from 20 to 612 amino acids (2); a seven-transmembrane domain (613-862) (18) and an intracellular tail of 216 amino acids (19), which participates in conveying extracellular stimuli into intracellular signaling pathways. While efforts to obtain pure ECD protein have been reported by two independent groups (20,21) using an HEK293 cell line stably transfected with the CaSR ECD and insect cells expressing the CaSR ECD, respectively, the structure of CaSR remains undetermined to date.

Our lab has built an homology model of the CaSR ECD based on the crystal structure of metabotropic glutamate receptor 1 (mGluR1) (22-24) and identified five potential Ca^{2+}-binding pockets using computational algorithms developed

in our lab (22,23). Using site-directed mutagenesis and intracellular Ca^{2+} readout, we further verified the roles of those predicted Ca^{2+}-binding sites and an L-Phe-binding site in regulating functional activities of the receptor (24).

Despite extensive functional studies on the CaSR by different groups (12,15,25-27), how calcium and L-Phe directly interact with the extracellular domain is still under debate due to the lack of structural information as well as absence of binding assays for sites with weak binding affinities (0.1-30 mM). One of several challenges is related to the high level of glycosylation in the CaSR ECD that not only increases the size of the protein but introduces structural heterogeneity into the entire system. Direct visualization of interactions of weak binding ligands with a receptor's ECD may also be hampered by the high off rate associated with weak binding. For example, Ca^{2+}-binding sites of mGluRs are not visible in all reported X-ray structures (28). Direct monitoring of ligands (Ca^{2+} and L-Phe) and protein interactions in solution and characterization of the biophysical properties of such a large protein as well as collection of structurally related information using spectroscopic methods also requires a large amount of homogenous native protein.

In the present study, we report our progress in expression and purification of the glycosylated extracellular domain of CaSR (ECD) (residues 20~612) using two mammalian expression systems that generate distinct glycosylated products, wild type 293-F cells or the HEK293S (GnTI⁻) cell line. The former wild type cell line generates recombinant products harboring heterogeneous complex type *N*-glycans. In contrast, the second HEK293S (GnTI⁻) cell line lacks the enzyme GlcNAc transferase I (GnTI) (29), an enzyme required for the first step in the conversion of high mannose *N*-glycans into complex and hybrid structures (30,31). The HEK293S (GnTI⁻) cells are unable to synthesize complex and hybrid N-glycans and instead produce oligosaccharides containing a more homogeneous collection of structures based on $Man_5GlcNAc_2$-Asn (32).

Here, a soluble, secreted form of the CaSR ECD was generated in 293-F or HEK293S (GnTI⁻) cells

by transient transfection, and the protein was further purified by affinity chromatography. The biophysical properties of the native CaSR ECDs were characterized using fluorescence titration spectroscopy, circular dichroism, and NMR spectroscopy. We demonstrate herein that the ECD of CaSR directly interacts with Ca^{2+} and L-Phe, with binding affinities in the mM range for both.

MATERIALS AND METHODS

Construct CaSR-ECD cDNA: For engineering of the CaSR-ECD, the sequence Tyr[20]-Phe[612] was cloned from CaSR-pCDNA 3.1(+) by standard PCR methods using the following 5' primer (CCGGAAT TCTACGGGCCAGACCAGCGAG CCCAA) and 3' primer (CCCAAGCTTTT AAAAGGGCTCCGTCCACGACAGAAACT). The cloned sequence was then inserted into the plasmid pGEn1 between the *Eco*RI and *Hin*dIII restriction sites. The engineered protein contains a signal peptide (MRLLTALFAYFIVALI LAFSVS AKS) followed by a His-tag and a StrepII tag at the N-terminus. A flag-tag site was inserted between residues D371 and T372. The plasmid constructs were confirmed by DNA sequencing (GENEWIZ, South Plainfield, NJ).

Protein expression and purification: For mammalian expression, either wild type HEK293 cells in suspension culture (FreeStyle 293-F cells, Life Technologies, Grand Island, NY) or mutant HEK293S GnTI- cells (29) (ATCC cat. no. CRL-3022) were transfected with pGEn1-hCaSR-ECD plasmid using the polyethyleneimine (PEI) method as previously described (33). The hCaSR-ECD was secreted into the culture media and harvested after centrifugation 3 times at 1500xg for 10 min. The supernatant was diluted with the following buffer, 75 mM Tris HCl, 360 mM NaCl, pH 8.0, at a ratio of 1:2 and further filtered through a 0.45 µm filter (Millipore, Billerica, MA). The filtered medium was applied to a 16/10 HisPrep HP column (GE Healthcare) pre-equilibrated with Buffer A (50 mM Tris HCl, 150 mM NaCl, 20 mM imidazole), and a linear segmented gradient of 0–100% Buffer B (50 mM Tris HCl, 500 mM NaCl, and 500 mM imidizole, pH 7.4) was run to elute the protein. The enriched protein was further treated with a desalting column (GE HiTrap) using 10 mM Tris Buffer (pH 7.4). The concentrations of hCaSR-ECD were determined using the BioRad protein assay.

Lectin Agarose Binding Assay: Fractions containing the CaSR ECD following HisPrep chromatography were mixed with 30 µL of RCA-1 lectin agarose (Vector Lab, Burlingame, CA) for overnight incubation at 4℃ followed by washing with PBS. The ECD protein was eluted using 0.2 M galactose. The eluted fractions were analyzed by Western blot, using an anti-flag antibody.

Deglycosylation reactions: Triton X-100 was added to heat- and SDS-denatured, purified ECD protein (20 µg) at a final concentration of 2% before the protein was subjected to the Peptide -N-Glycosidase F (PNGase F) deglycosylation procedure. Approximately 1.4 units of PNGase F were added per microgram of purified protein and incubated for 2 h at 37℃. The deglycosylated samples were further analyzed by Western blot using the anti-Flag antibody. For Endoglycosidase F1 (Endo F1) enzyme treatment under native conditions, purified CaSR-ECD protein generated in HEK293S (GnTI-) cells was taken directly from the appropriate FPLC fractions and incubated with Endo F1 at a mass ratio 1:3 in 10 mM Tris buffer, pH 7.4 for overnight incubation at 4 ℃.

Circular Dichroism: The circular dichroism spectra were recorded from 190 to 260 nm on a Jasco-810 spectropolarimeter purged by N_2 and equipped with a temperature control system (CTC-345). Spectral and temperature-dependent measurements were performed at a bandwidth of 2 nm using a U-type quartz cell of path length 0.1 mm with protein concentrations ranging from 8 to 10 µM in 10 mM Tris-HCl, pH 7.4. Five spectra

were recorded for each sample at a scan rate of 50nm/min and response time of 1s. The continuous temperature dependence of the ellipticity at 222 nm was measured using a scan rate of 50 °C/h and a delay time of 100 s. The cuvette was sealed with parafilm to prevent solvent evaporation.

The spectra were deconvoluted using the Selcon method after subtracting the spectrum of the buffer as the blank, and the CD data are depicted in units of molar ellipticity per residue. The melting curve was fitted using the equation

$$\Delta S = \Delta S_{max}/(1 + e^{(T_m-T)/k}) \quad (Eq1)$$

to obtain the thermal transition point, where ΔS and ΔS_{max} are the signal changes at each data point and the final point; T_m and T are the transition temperature and experimental temperature, respectively. k is a transition rate that defines how fast the temperature-induced change occurs, which is represented by the slope of the transition phase in the fitting curve. A smaller k results in a sharper transition (34).

Fluorescence Spectroscopy: A Photon Technology International (Edison, New Jersey) Lifetime Fluorimeter was used to record the fluorescence spectra at room temperature using a 1-cm path length cell. Intrinsic tryptophan emission spectra were recorded from 300 to 400 nm with an excitation wavelength at 282 nm. The slit widths were set at 0.3~1 nm for excitation and 1.0~2.0 nm for emission, respectively. The calcium titration was performed in a buffer system (10 mM HEPES, 120 mM NaCl and 10 mM KCl, pH=7.2) with protein concentrations of 1.5~2.0 μM by adding a known amount of $CaCl_2$. The free Ca^{2+} concentration in the buffers used in this study, which were not treated with Chelex-100, has been measured to be <10 μM using BAPTA, a calcium-specific chelator. Our previous studies showed that the Ca^{2+} dissociation constant was determined to be ~0.7 mM for the "high affinity"

Ca^{2+}-binding site (22). Given this fact, the background Ca^{2+} concentration may be negligible. For the Tyr/Trp-sensitized Tb^{3+} fluorescence energy transfer (Tb^{3+}-FRET) assay, protein samples (1.5~2.0 μM) were in 20 mM PIPES-10 mM KCl at pH 6.8. The emission spectra were collected from 500-600 nm with the excitation at 282 nm. The slit widths for excitation and emission were set at 1 nm and 3 nm, respectively. Secondary Rayleigh scattering was circumvented by using a glass filter with a cutoff of 320 nm. The Tb^{3+} titration was performed by adding various volumes of Tb^{3+} stock solutions (1 mM) stepwise into the cuvettes. The Ca^{2+} -Tb^{3+} competition experiments were performed in solutions containing 30~50 μM Tb^{3+} and 2 μM protein as the starting point. The stock solutions of 100 mM or 1 M $CaCl_2$ with the same concentration of Tb^{3+} were gradually added into the mixture. The background fluorescence intensity was subtracted using logarithmic fitting and the Tb^{3+}-binding affinity of the protein was calculated by fitting normalized fluorescence intensity data using the

Hill equation $\Delta S = \dfrac{[M]^n}{K_d^{\,n} + [M]^n}$ (Eq.2)

where ΔS is the total signal change in the equation, K_d is the apparent binding affinity, n is the Hill coefficient, and [M] is the free metal concentration.

The Ca^{2+} competition data were first analyzed to derive the apparent dissociation constant by Equation 3. By assuming that the sample is saturated with Tb^{3+} at the starting point of the competition, the Ca^{2+}-binding affinity is further obtained by using the equation,

$$K_{d,Ca} = K_{app} \frac{K_{d,Tb}}{K_{d,Tb} + [Tb]} (Eq. 3)$$

where $K_{d,Ca}$ and $K_{d,Tb}$ are the dissociation constants of Ca^{2+} and Tb^{3+}, respectively. K_{app} is the apparent dissociation constant.

ANS-Binding Measurements: For the ANS (8-anilino-1-naphthalenesulfonic acid) binding assay, protein samples were incubated with a buffer containing 40 μM ANS, 50 mM Tris-HCl and 100 mM KCl (pH 7.4) with either 5 mM EGTA or 3 mM Ca^{2+} at 4°C in the dark for 1 h with constant rotation prior to measurements. The excitation wavelength was set at 370 nm, and the emission spectra were acquired from 400 to 600 nm. For the Ca^{2+} titration, the protein concentration was 2.0 μM and the Ca^{2+} concentration was varied from 0 to 30 mM in 20 mM Tris-HCl, 50 mM KCl, pH 7.4.

NMR Spectroscopy of CaSR ECD: All NMR spectroscopy experiments were performed on a VARIAN Inova 800 MHz spectrometer equipped with the cryogenic HCN probe at 37 °C. The CaSR-ECD was prepared in 10 mM Tris, pH 7.4, 20% (v/v) D_2O for NMR experiments. For the calcium titration, both one dimensional ^1H and two-dimensional ^1H-^{15}N NMR spectra of ^{15}N-Phe selectively labeled CaSR-ECD in the presence of 0, 1, 3, 5 and 10 mM Ca^{2+} were collected and processed by MestReNova (35) and NMRpipe (36), respectively. The ^1H-^{15}N-HSQC data were analyzed by Sparky (37) and the chemical shift perturbations were calculated using the equation

$$\Delta\delta_{av} = \sqrt{0.5\times[(\Delta\delta^1H)^2 + 0.07\times(\Delta\delta^{15}N)^2]} \text{ (Eq.4)}$$

where $\Delta\delta_{av}$ is the chemical shift perturbations of the ^1H-^{15}N spectra, $\Delta\delta$ is the chemical shifts for ^1H or ^{15}N (38).

For STD-NMR, 20 μM CaSR-ECD expressed in HEK293S (GnTI-) cells was prepared in 10 mM Tris in D_2O, pD 7.8. The blank experiment without protein was performed to examine the absence of direct saturation of L-Phe in certain on-resonance frequencies. Saturation transfer from the protein to L-Phe was achieved by irradiating at -1 ppm with a duration of 3 s. The reference spectra were obtained by irradiating at 30 ppm. The STD-NMR data were processed and analyzed by MestReNova

and the STD amplification factor was calculated by using the equation

$$STD-AF = \frac{I_{ref} - I_{sat}}{I_{ref}} \times \frac{[L]_T}{[P]} \text{ (Eq.5)}$$

where AF stands for amplification factor.

The K_d was determined using the equation

$$STD-AF = \frac{\alpha_{std}[L]}{K_D + [L]}, \text{ (Eq. 6)}$$

where α_{std} is the amplification when it is saturated by a ligand (39).

Statistics: The data are presented as means $\pm$ SE of three independent experiments. Statistical analyses were carried out using the unpaired Student's t-test when two groups were compared. A P value of < 0.05 was considered to indicate a statistically significant difference.

RESULTS

The CaSR ECD forms a dimer in culture medium: Wild type 293-F cells or HEK293S (GnTI-) cells were transiently transfected with engineered CaSR ECD cDNA (Fig.1a). The signal peptide at the N-terminus led to secretion of the CaSR ECD (Fig. 1b), which is predicted to have five potential Ca^{2+}-binding sites based on the homology model of metabotropic glutamate receptor 1 (mGluR1) (Fig. 1c), into the culture medium. (22). These His-tagged CaSR ECDs were efficiently separated from other proteins with a HisPrep column using an imidazole gradient (Fig. 2 a and b). The fractions containing CaSR ECD were collected and separated by SDS-PAGE under reducing conditions (Fig. 2 a and b). Immunoblots were further applied to visualize the CaSR in the samples using specific anti-CaSR antibody. As shown in Fig. 2 (panels c-e) CaSR ECD from 293-F cells exhibited a diffuse band in the range from ~100 to ~130 kDa suggesting heterogeneity of glycosylation while the GnTI- CaSR has a single

sharp band with a molecular weight of approximately 95 kDa. The non-reducing samples from the 293-F cells and the GnTI⁻ cells expressing the CaSR ECD have molecular weights at around 240 kDa and 200 kDa, respectively, corresponding to the respective calculated molecular weights of the dimerized forms of the receptor extracellular domain.

The secreted CaSR ECD is glycosylated: In order to verify that the secreted 293-F CaSR ECD is glycosylated, Ricinus Communis Agglutinin I (RCA I) agarose beads, which preferentially bind to complex oligosaccharides, were incubated with the purified protein. The CaSR ECD expressed in 293-F cells interacted with the RCA I beads (Fig. 2f) and high concentrations of galactose (200 mM) competed with the glycoprotein for interaction with the lectin agarose beads. Peptide *N*-glycosidase F (PNGase F) cleaves high mannose, hybrid, and complex oligosaccharides from *N*-linked glycoproteins between the innermost acetylglucosamine (GlcNAc) and the underlying asparagine residues (40). Cleavage of denatured CaSR ECD generated in 293-F cells with PNGase F resulted in a decrease from ~100 to ~ 80 kDa (Fig. 2g) indicating that the protein is highly glycosylated. Similarly, Endo F1 cleaves between the two core GlcNAc residues on high mannose, but not hybrid or complex type *N*-glycans to leave a single GlcNAc residue attached to the polypeptide (41). Cleavage of the CaSR ECD derived from HEK293S (GnTI-) cells with Endo F1 under non-denaturing conditions resulted in the production of a lower molecular weight band at ~ 87 kDa in the reducing SDS-Page gels, which indicates that this recombinant product contains exclusively high mannose N-glycans.

Measuring the secondary and tertiary structure of CaSR ECDs: In order to analyze the secondary structures of the purified CaSR ECDs, circular dichroism measurements were performed. Typical far-UV CD spectra for both protein preparations are shown in Fig. 3. Analysis of all the spectra indicated that the purified 293-F and GnTI⁻ CaSR ECD shared similar secondary structures with α helical contents of 52-58% and β-sheet contents of 17-25%. The addition of calcium produced minimal changes in the spectra of either the 293-F CaSR ECD or the GnTI⁻ CaSR ECD (Fig. 3a and b, Table 1).

The tryptophan environment and the packing of proteins can be monitored by analyzing the intrinsic tryptophan emission spectra at 300 to 400 nm using an excitation wavelength of 282 nm, since there are twelve tryptophan (Trp) residues in the ECD. The emission spectrum of free Trp has a peak at around 350 nm. The emission peak undergoes a blue-shift if the tryptophan is embedded in a hydrophobic environment. All the Trp emission spectra of the various forms of the CaSR ECD showed a peak at around 334 nm indicating that the proteins have retained their native-like structure (Fig. 4).

The Stability of CaSR ECDs: The stabilities of the purified ECDs were further investigated using immunoblots. Samples of the CaSR ECD from both 293-F and the HEK293S (GnTI⁻) cells were kept at room temperature continuously for seven days without any appreciable loss of protein from degradation as assessed by Western blots (Fig. 3 d and e). The proteins were subjected to stepwise increases in temperature to measure their thermal stability. The molar ellipticity signal was monitored from 4~ to 95 °C at 222 nm. As shown in Fig. 3c, the 293-F CaSR ECD demonstrated extraordinary thermal stability as the signal at the given wavelength did not change in this temperature range. The high mannose form of the CaSR ECD from HEK293 (GnTI⁻) cells appeared to be slightly less stable with an increase in ellipticity at > 92°C. The cooperative unfolding transition further support the formation of a well-packed core for the CaSR ECD as revealed by Trp emission fluorescence. The effect of calcium on the thermal stability was not determined due to

precipitation of the protein at high temperature in the presence of calcium.

The effect of calcium-binding on CaSR ECDs: As shown in Fig. 3 a and b, the addition of Ca^{2+} leads to small changes in the secondary structure of CaSR ECDs as revealed by CD. However, the addition of Ca^{2+} could possibly induce more significant local conformational changes as probed by various spectroscopic methods.

Ca^{2+}-induced conformational changes were probed by both Trp and ANS emission spectra (Fig. 4 and 5). Binding of Ca^{2+} resulted in a 2~3 nm blue shift of the emission maxima of the Trp fluorescence spectra of both the 293-F CaSR ECD and the HEK293S (GnTI⁻) CaSR ECD. Furthermore, a 20% decrease in the Trp fluorescence intensity of the CaSR ECD expressed in 293-F cells was observed upon addition of saturating amounts of Ca^{2+}, whilst 14% decreases in the signal were shown in the case of the CaSR ECD expressed in HEK293S (GnTI⁻) cells. The K_d of Ca^{2+} determined by Trp florescence changes of CaSR was 4.9 ± 0.3 mM and 5.4 ± 0.2 mM for 293-F CaSR ECD and GnTI⁻ CaSR ECD, respectively. The Hill coefficients obtained from the Trp fluorescence spectra were 1.3 ± 0.1 for 293-F CaSR ECD and 1.1 ± 0.1 for GnTI⁻ CaSR ECD, indicating the two protein variants differing in glycosylation may share similar Ca^{2+} binding capability (Fig. 4 and Table 2), although the Hill number obtained by this method is substantially lower than that obtained by functional assays (~3-4)

ANS, a fluorescence probe extensively used for the detection and analysis of protein conformational changes, was applied to the study of the two proteins (42). Fig. 5 shows that addition of either form of the CaSR ECD resulted in a 30 nm blue shift of the spectra of ANS dye from 500 to 466 nm and a 10-fold increase in fluorescence intensity (Fig. 5). Such a blue shift of the emission spectrum and increase of the fluorescence intensity

suggest that the fluorophore is located in less polar media (43).

Interestingly, Fig. 5 shows that Ca^{2+} also induced greater exposure to solvent of more hydrophobic regions in the complex oligosaccharide form of the ECD (293-F CaSR ECD) that was indicated by a 25% increase in the fluorescence signal intensity contrasting with the 10% change in intensity for the high mannose glycosylated form of the ECD expressed in HEK293S (GnTI⁻) cells. The calcium-induced ANS florescence signal at 466 nm was also fitted by the Hill equation. The 293-F CaSR ECD had a K_d of 3.8 ± 0.2 mM while GnTI⁻ CaSR ECD had a K_d value at 3.2 ± 0.1 mM. Their corresponding Hill coefficients calculated from the Ca^{2+}-ANS titration curves were 2.6 ± 0.2 and 2.3 ± 0.2 respectively (Fig. 5 & Table 2). This approach, therefore, may sample more Ca^{2+}-binding sites than the use of Trp fluorescence.

Due to their similarities in ionic radii and coordination chemistries, Tb^{3+} has been commonly used to probe Ca^{2+}-binding sites as a trivalent Ca^{2+} analogue. There are 12 Trp residues on the CaSR ECDs. According to the model structure of the CaSR ECD, several Trp residues are within 10 Å of these potential calcium-binding pockets, thus enabling aromatic residue-sensitized Tb^{3+}-luminescence resonance energy transfer (LRET). Fig. 6 shows that titration of Tb^{3+} into a solution containing either of the two ECDs showed an enhanced LRET (Fig. 6), consistent with Tb^{3+}-binding in close proximity to the predicted calcium-binding sites. On the other hand, addition of calcium to the Tb^{3+}-bound ECDs resulted in a decrease of the fluorescence signal indicating competition between the two ions (Fig. 7). The Tb^{3+}-binding affinity for 293-F CaSR ECD was about 36.6 ± 0.4 μM with a Hill coefficient at 1.2 ± 0.1 suggesting a 1:1 binding mode of the interaction between Tb^{3+} and its binding pockets (Fig. 6). In terms of GnTI⁻ CaSR ECD, the K_d for Tb^{3+} was 31.8 ± 0.3 μM which is comparable with the 293-F CaSR ECD. The Ca^{2+}-Tb^{3+} competition

7

assay yielded apparent dissociation constants for the ECDs, from which the binding constants for calcium can be deduced (Fig.7). The Ca^{2+}-binding dissociation constants calculated from Ca^{2+}-Tb^{3+} competition assay using equation 2 for the 293-F CaSR ECD and the GnTI- CaSR ECD were 3.7 ± 0.2 mM and 2.4 ±0.2 mM, respectively, which are comparable to the K_d calculated from Ca^{2+}-induced changes in native Trp signals as well as the ANS spectra.

Perturbations of NMR chemical shift can be used to monitor the interactions between metals and the protein. To ascertain whether those perturbations are occurring at the interacting interface of the ECD with its large protein size, we achieved specifically labeling of Phe residues with ^{15}N in both mammalian expressed proteins with a yield of 4-5 mg/L and 0.9-1.0 mg/L for 293F cells and GnTI- cells, respectively (MATERIALS AND METHODS). Both of the ^{15}Phe-labeled proteins exhibited identical native dimer conformations similar to the unlabeled proteins (Fig. 2).

The low resolution of the peaks didn't permit assignment of the chemical shifts of the high mannose form of the protein. Ca^{2+}-induced protein conformational change could be observed in the one-dimensional (1D) NMR when Ca^{2+} was titrated into the ^{15}N L-Phe-labeled 293-F CaSR ECD (Fig. 8). The Ca^{2+} induced changes in two-dimensional (2D) NMR could be evaluated using 293-F CaSR ECD. As shown in Fig. 9, during the titration with Ca^{2+}, a progressive disappearance of the amide signals at 8.05 ppm was accompanied by the concomitant emergence of a new set of peaks at 7.85 ppm as well as a chemical shift between the amide signals at 7.95 ppm and 8.21 ppm (Fig. 9a, b, and c) indicating a complex response to Ca^{2+}-binding. The low expression yield and dispersion of the ^{15}N Phe-labeled GnTI- CaSR ECD with high mannose form prevented us from further studies using NMR.

The chemical shifts of the peaks were further plotted as calcium concentration-response curves as shown in Fig. 9 (right panel). The calcium-induced chemical shift changes at 8.18 and 7.96 ppm with intermediate and fast exchanges in Fig. 9b could be well-fitted by the Hill equation assuming formation of a 1:1 ligand-protein complex with a K_d of 1.1 mM (Fig. 9 upper right panel). On other hand, analysis of the peaks in Fig. 9c suggests a slow exchange process in which the exchange rates of the bound and unbound conformations were slower than the change in amide chemical shifts in frequency units. The Ca^{2+} concentration-response curve with a K_d at 2.5 mM and a Hill coefficient of 2.5 suggesting more than one ligand-binding site, and similar to the values obtained using the ANS assay

L-Phe modulated the binding of Ca^{2+} to CaSR by directly interacting with the CaSR ECDs. Direct evidence demonstrating the interaction between this amino acid with the CaSR ECD is difficult to achieve due to the dynamic binding process, weak binding affinity and sample limitation. We have applied saturation transfer difference (STD) NMR, a widely used NMR technique, to facilitate the exploration of low affinity protein-ligand interactions (10^{-8}~10^{-3}) due to the fact that it detects the signals from the ligands via saturation transfer between the protein protons and the ligand protons (44). Only small amounts of non-labeled proteins or macromolecules are required. As shown in Fig. 10a, we observed that an intense proton signal around downfield 7.2 ppm that increased upon addition of 1 mM L-Phe (green line), which corresponds to the characteristic ^1H L-Phe NMR spectrum. The three major peaks in the STD spectrum of L-Phe (red line) are from the protein signal from the ECD of CaSR. The STD-AF signal obtained by integrating each peak was plotted against the L-Phe concentration and was further fitted to the Hill equation (Fig. 10 b and c). A lower STD-AF signal was observed from interaction of the amino acid, L-Asp, with the

protein (Fig. 10 e), which was correlated with the weaker capacity of L-Asp to activate the receptor compared with L-Phe in intact cells (12). These spectra provide direct evidence to support the earlier hypothesis that L-Phe can bind to the extracellular domain of the calcium-sensing receptor with a K_d at 10.2 mM and a Hill coefficient of 1.4 (Fig. 10 b and c). Quantification of the STD-AF signal indicated that the binding constant of L-Phe to the GnTI⁻ CaSR ECD was decreased to 4.6 mM with a Hill coefficient of 1.8 in the presence of 3.2 mM calcium, which is the calculated K_d of GnTI⁻ CaSR ECD for calcium. We also demonstrated in the current study that addition of 10 mM L-Phe also decreased the K_ds for the binding of calcium to the 293-F ECD and the GnTI-ECD from 4.9 ± 0.3 mM to 3.2 ± 0.3 mM and 5.4 ± 0.2 mM to 3.4 ± 0.3 mM, respectively (Fig. 4 c and d). These results suggest that the interaction between Ca^{2+} and the receptor may influence the binding between L-Phe and the CaSR ECD and vice versa (Fig. 10 c and d).

DISCUSSION

The secreted CaSR ECD variants maintain native-like structural properties: In the present study, we were able to purify CaSR ECDs from both a wild type mammalian expression host using 293-F cells, to generate complex type *N*-glycan structures, as well as from the HEK293S (GnTI⁻) cell line to produce high mannose *N*-glycans on recombinant products. In both of the two host cell systems, the target proteins were secreted into the culture media due to the presence of a signal peptide at the beginning of the ECD sequence. We have performed several studies to support the conclusion that the secreted ECD variants with different types of glycosylation maintain their native structural and functional properties.

First, the secreted ECD proteins containing either the complex or high mannose glycans both appear to form dimers in the culture medium (Fig 2)

consistent with the fact that CaSR functions as a dimer on the cell surface (45).

Second, the secreted recombinant CaSR ECD containing complex glycosylation is able to bind to RCA-I beads and is susceptible to cleavage with PNGase F. Similar data were obtained for the EndoF1 cleavage of the high mannose N-glycans from the ECD produced in HEK293S (GnTI⁻) cells under native conditions (Fig. 2f). The above evidence suggests that the secreted proteins from the mammalian cell lines maintain their glycosylated characteristics.

Third, far UV CD analysis of the two glycosylated forms of CaSR suggests that both have similar secondary structure contents, with 52-58% α helical contents and 17-25% β-sheet contents. These results are consistent with the modeled structure based on mGluR1's crystal structure (Table 1) (46,47).

The well-formed tertiary structure with a hydrophobic core of the secreted ECD of CaSR was revealed by a Trp emission maximum at 332 nm (Fig. 4). The highly stable ECD protein with complex type saccharides was able to maintain its secondary structure at high temperature (>90°C), while the CaSR ECD with its high mannose glycans was slightly less stable, exhibiting cooperative thermal unfolding. Such strong thermal stability and unfolding behavior are likely due to the formation of a stable hydrophobic core and the existence of well-formed, multiple disulfide bonds in the CaSR ECD (48).

Ca^{2+} directly interacts with the extracellular domain of CaSR: We have used various spectroscopic methods to demonstrate the capacities of Ca^{2+} and Phe to bind to the ECD variants of CaSR studied here (Figs 4, 5, 8, 9 and 10). As summarized in Tables 2 and 3, both variants exhibit similar Ca^{2+}-binding despite the different methods that were employed.

9

The K_ds for the interactions of Ca^{2+} with the ECDs that were monitored by intrinsic Trp florescence were 4.9 ± 0.3 mM and 5.4 ± 0.2 mM for the ECDs from 293-F and GnTI$^-$ cells, respectively. The K_ds based on ANS florescence enhancement were 3.8 ± 0.2 mM and 3.2 ± 0.1 mM for the ECDs from the same respective cell lines. The Ca^{2+}-K_ds based on Tb^{3+} competition in FRET analysis were 3.7 ± 0.2 mM and 2.4 ± 0.2 mM for 293-F and GnTI$^-$ cells, respectively, and similar millimolar binding constants were determined from chemical shifts in NMR spectra. These data indicate that Ca^{2+} can bind to the ECD of CaSR with a K_d in the mM range and that the alterations in glycosylation do not significantly alter the binding of Ca^{2+} to the ECD.

Functional studies of the CaSR in cells as well as our previous metal-binding studies using grafting approaches have demonstrated that the CaSR likely has multiple Ca^{2+}-binding sites (49). The Hill coefficients of both the 293-F and GnTI$^-$ CaSR ECDs calculated from calcium-induced ANS spectral changes (2.3~2.6) were also in agreement with the multiple Ca^{2+}-binding modes. However, the intrinsic tryptophan spectral changes during the Ca^{2+} titration indicated mono- to biphasic binding of Ca^{2+} to CaSR with Hill coefficients in the range of 1.4~1.6. The discrepancy might be attributed to differences in the principles underlying the experiments. 7 out of 10 tryptophan residues in the CaSR ECD are predicted to be located in lobe 2. Of all of these ten Trp residues, two of them (Trp[70] and Trp[299]) are within 10 Å of calcium-binding site 1. Although Trp[208] is close to calcium-binding site 3 (~ 10 Å) and Trp[352] is nearby calcium--sites 4 and 5 (< 10 Å), both of which are more than 20 Å from site 1. Thus, the "sampling" of site 1 by Trp fluorescence may be more efficient than that of the others because site 1 may produce signals arising from 2 Trp, while the other sites are only close to one Trp each. Future studies could utilize site-directed mutagenesis of sites 1-5 to determine

which one(s) contribute most to Ca^{2+}-induced changes in Trp fluorescence and the other spectroscopic methods used here to assess Ca^{2+}-binding.

In previous studies from our lab, CaSR ECD subdomain 1, which includes predicted Ca^{2+}-binding sites 1, 2 and 3, showed biphasic binding processes when titrated with Tb^{3+}, while subdomain 2 (including Ca^{2+}-binding site 2 and 3) and subdomain 3 (including Ca^{2+}-binding site 4 and 5) had monophasic responses to Tb^{3+}. However, in the present studies, the Tb^{3+}-concentration response curve for the 293-F and GnTI$^-$ CaSR ECDs did not show observable cooperative binding. This could possibly be due to the fact that in the grafting approaches, the subdomains were not constrained by the additional structural conformations that might be present when they are in the intact ECD structure. Concomitantly, the CaSR ECDs had much stronger binding affinities for Tb^{3+} than Ca^{2+} with K_ds at μM range. Thus, the differences of ligand binding capacity between potentially weak metal-binding sites may not be detected. Moreover, intensive FRET signals between Tb^{3+} and more than one Trp residue in the intact ECD, as for site 1, might produce a strong signal that could obscure possible cooperativity among these metal binding sites. On the contrary, fitting the data from the ANS assay resulted in Hill coefficients of >2. These data indicate that the ANS assay may provide a more effective means of capturing both local and global conformational changes in CaSR ECDs resulting from Ca^{2+} interacting with multiple binding sites. These results from the ANS assay are in accordance with the observed multiple binding states from NMR spectra as shown in Fig. 9. Thus the different methods used here to assess Ca^{2+}-binding to the two forms of the ECD studied here may differ in their capacity to "capture" cooperativity between Ca^{2+}-binding sites. This might be the result of differences in their capacities to detect and "sample" the various

predicted and other possible Ca^{2+}-binding sites within the ECD to an equivalent extent. Studies in intact cells, in contrast, integrate the overall signal resulting from cooperative binding of Ca^{2+} to its various sites in the ECD and perhaps elsewhere.

Dynamic interaction of L-Phe to CaSR: Several studies from our laboratory and others have shown that L-Phe potentiates intracellular Ca^{2+} oscillations and other responses using site-directed mutagenesis and functional studies with HEK293 cells expressing the CaSR (12,24,27,50). *In vivo* studies suggest that a minimum of 1 mM calcium is required in extracellular buffers in order to detect the L-Phe-triggered changes in intracellular Ca^{2+} concentration (15). While the Phe binding site of CaSR has been proposed to be located on the ECD, direct binding of Phe to CaSR has never been reported. In the present study we confirmed a direct interaction between the extracellular domain and this CaSR allosteric regulator in the absence of Ca^{2+} using the STD NMR techniques with a binding affinity of 10.1 mM and a Hill coefficient of 1.4. Since L-Phe activates CaSR though signaling pathways in addition to $[Ca^{2+}]_i$ signaling, the difference between the binding constant of L-Phe determined here and its EC_{50} in intact cells might be attributable, at least in part, to the synergistic effect of multiple downstream effects in cells (15,51).

L-Phe and Ca^{2+} mutually facilitated each other's interaction with the CaSR ECD. Several studies in intact cells have revealed that the EC_{50}s of CaSR for binding of extracellular Ca^{2+} could be reduced from 4.0 mM to 2.5 mM in the presence of L-Phe (12,24). Here, we demonstrated that L-Phe also increased the binding affinity of Ca^{2+} to the CaSR ECD measured directly using spectroscopic methods. Namely, 10 mM L-Phe reduced the K_ds for Ca^{2+}-binding from 4.9 $\pm$ 0.3 mM to 3.2 $\pm$ 0.3 mM for 293-F ECD and from 5.4 $\pm$ 0.2 mM to 3.4 $\pm$ 0.3 mM for GnTI- ECD (Fig. 4 c and d).

Meanwhile, the presence of Ca^{2+} also increased the binding affinity of L-Phe to CaSR ECD, reducing the K_d from 10.2 mM to 4.6 mM. Similarly, functional studies carried out by Conigrave *et al*. in intact cells demonstrated that the half-maximal effect of L-Phe (EC_{50}) was 3.5 mM in the presence of Ca^{2+} (12). These results provide evidence that potentiation of the activity of CaSR by L-Phe is at least partially exerted through its direct interaction with the extracellular domain. The intensity of the L-Phe STD signal was decreased in the presence of Ca^{2+} compared to that in the absence of Ca^{2+}. It is possible that the conformation of the ECD was altered upon binding Ca^{2+} so that it can better accommodate L-Phe. Thus, the proton signal from L-Phe was not reflected as a simple additive effect on the STD spectrum when Ca^{2+} was added in the system. It is also possible that the agonist-induced change in receptor conformation involves intermolecular reorientation of the receptor at the dimer interface. In fact, in the case of the crystal structures of mGluR1(1EWT, 1EWK, 1ISR), binding of glutamate produced not only domain closure but also a small shift of an α helix at the dimer interface along with a substantial rotation around the axis between the two ECDs (52).

Ligand- induced conformational changes of the ECD of CaSR: Ca^{2+}-induced conformational changes in the intact CaSR ECD were observed in both fluorescence and NMR spectra. There are seven tryptophan residues on the ECD, and among these are four that are proposed to be on the molecular surface between lobes 1 and 2. As Ca^{2+} bound to the protein, the polarity surrounding the tryptophan residues increased leading to a decreased fluorescence signal from the emission spectra. On the other hand, the signal from the ANS spectrum increased upon titration of Ca^{2+} suggesting the presence of ligand-induced exposure of more hydrophobic regions of the protein to interact with the ANS probe. The increase in the Ca^{2+}-induced ANS signal of the 293-F CaSR ECD was larger than that observed

with the GnTI⁻ CaSR ECD, which indicates that the glycans on the 293-F CaSR ECD might contribute to the changes in hydrophobicity of the protein triggered by Ca^{2+}.

Calcium-induced alterations in conformation were also monitored by NMR chemical shift changes using uniform ^{15}N-Phe labeled 293-F CaSR ECD (Fig. 9). Chemical shifts of several Phe residues displayed differential behavior upon addition of calcium, indicating alterations in the local environments around these Phe residues. There are more than 30 phenylalanine residues in the ECD of CaSR; however, a limited number of peaks were detected using 900MHz NMR, which precluded further assignment. Currently, we are working on labeling and assignment strategies to enable further structural studies by high resolution NMR.

The observed ligand-induced conformational changes of the CaSR ECD are fundamental initial signals that initiate intracellular signaling via multiple downstream molecules leading to the regulation of parathyroid hormone (PTH) secretion and numerous other biological processes. Such interactions likely to be shared by other members of family C of the GPCRs. Several

research articles have reported ligand bound forms and unliganded forms of mGluRs, showing alterations in the bi-lobed protomer architecture between the active and resting status through the modulation of the dimeric interface through a packed α-helical structure (47,52,53). Ligands stabilize mGluR1 in the active form by keeping the closed bi-lobed receptor structure as the dominant state in dynamic equilibrium (47). Interestingly, our previous work also elucidated a potential Ca^{2+}-binding site adjacent to the glutamate -binding site located at the hinge region of the ECD of mGluR1(28). Overall, the present study correlates well with observations from *in vivo* studies in intact cells using an intracellular Ca^{2+} readout (24), and will provide further insights into the structural underpinnings of agonist-induced functions of the CaSR. This work should also permit further studies to define the key residues on the receptor involved in the interaction with ligands, including cations (e.g. Ca^{2+}), nutrients such as amino acids, as well as antibiotics. This information will be crucial to understanding how the CaSR responds to variety of stimuli and may pave the way for future studies of other members of family C of the GPCRs.

REFERENCES

1. Brown, E. M., Pollak, M., and Hebert, S. C. (1998) The extracellular calcium-sensing receptor: its role in health and disease. *Annu Rev Med* **49**, 15-29
2. Brown, E. M., Gamba, G., Riccardi, D., Lombardi, M., Butters, R., Kifor, O., Sun, A., Hediger, M. A., Lytton, J., and Hebert, S. C. (1993) Cloning and characterization of an extracellular Ca^{2+}-sensing receptor from bovine parathyroid. *Nature* **366**, 575-580
3. Brown, E. M., and MacLeod, R. J. (2001) Extracellular calcium sensing and extracellular calcium signaling. *Physiological reviews* **81**, 239-297
4. Tfelt-Hansen, J., and Brown, E. M. (2005) The calcium-sensing receptor in normal physiology and pathophysiology: a review. *Crit Rev Clin Lab Sci* **42**, 35-70
5. Tfelt-Hansen, J., Schwarz, P., Brown, E. M., and Chattopadhyay, N. (2003) The calcium-sensing receptor in human disease. *Front Biosci* **8**, s377-390
6. Conigrave, A. D., Franks, A. H., Brown, E. M., and Quinn, S. J. (2002) L-amino acid sensing by the calcium-sensing receptor: a general mechanism for coupling protein and calcium metabolism? *European journal of clinical nutrition* **56**, 1072-1080

7. Chattopadhyay, N., Vassilev, P. M., and Brown, E. M. (1997) Calcium-sensing receptor: roles in and beyond systemic calcium homeostasis. *Biol Chem* **378**, 759-768

8. Cheng, I., Klingensmith, M. E., Chattopadhyay, N., Kifor, O., Butters, R. R., Soybel, D. I., and Brown, E. M. (1998) Identification and localization of the extracellular calcium-sensing receptor in human breast. *The Journal of clinical endocrinology and metabolism* **83**, 703-707

9. Chang, W., Tu, C., Chen, T. H., Komuves, L., Oda, Y., Pratt, S. A., Miller, S., and Shoback, D. (1999) Expression and signal transduction of calcium-sensing receptors in cartilage and bone. *Endocrinology* **140**, 5883-5893

10. Yazici, D., Ozben, B., Yavuz, D., Deyneli, O., Aydin, H., Tarcin, O., and Akalin, S. (2011) Epicardial adipose tissue thickness in type 1 diabetic patients. *Endocrine* **40**, 250-255

11. Riccardi, D. (2002) Wellcome Prize Lecture. Cell surface, ion-sensing receptors. *Exp Physiol* **87**, 403-411

12. Conigrave, A. D., Quinn, S. J., and Brown, E. M. (2000) L-amino acid sensing by the extracellular Ca^{2+}-sensing receptor. *Proc Natl Acad Sci U S A* **97**, 4814-4819

13. Quinn, S. J., Ye, C. P., Diaz, R., Kifor, O., Bai, M., Vassilev, P., and Brown, E. (1997) The Ca^{2+}-sensing receptor: a target for polyamines. *Am J Physiol* **273**, C1315-1323

14. Brown, E. M., Katz, C., Butters, R., and Kifor, O. (1991) Polyarginine, polylysine, and protamine mimic the effects of high extracellular calcium concentrations on dispersed bovine parathyroid cells. *J Bone Miner Res* **6**, 1217-1225

15. Breitwieser, G. E. (2006) Calcium sensing receptors and calcium oscillations: calcium as a first messenger. *Current topics in developmental biology* **73**, 85-114

16. Conigrave, A. D., Quinn, S. J., and Brown, E. M. (2000) Cooperative multi-modal sensing and therapeutic implications of the extracellular Ca^{2+} sensing receptor. *Trends in pharmacological sciences* **21**, 401-407

17. Ray, K., Clapp, P., Goldsmith, P. K., and Spiegel, A. M. (1998) Identification of the sites of N-linked glycosylation on the human calcium receptor and assessment of their role in cell surface expression and signal transduction. *J Biol Chem* **273**, 34558-34567

18. Garrett, J. E., Capuano, I. V., Hammerland, L. G., Hung, B. C., Brown, E. M., Hebert, S. C., Nemeth, E. F., and Fuller, F. (1995) Molecular cloning and functional expression of human parathyroid calcium receptor cDNAs. *J Biol Chem* **270**, 12919-12925

19. Magno, A. L., Ingley, E., Brown, S. J., Conigrave, A. D., Ratajczak, T., and Ward, B. K. (2011) Testin, a novel binding partner of the calcium-sensing receptor, enhances receptor-mediated Rho-kinase signalling. *Biochem Biophys Res Commun* **412**, 584-589

20. Goldsmith, P. K., Fan, G. F., Ray, K., Shiloach, J., McPhie, P., Rogers, K. V., and Spiegel, A. M. (1999) Expression, purification, and biochemical characterization of the amino-terminal extracellular domain of the human calcium receptor. *J Biol Chem* **274**, 11303-11309

21. Ryan, Z. C., Craig, T. A., Venyaminov, S. Y., Thompson, J. R., and Kumar, R. (2006) Biophysical properties of the extra-cellular domain of the calcium-sensing receptor. *Biochem Biophys Res Commun* **349**, 339-344

22. Huang, Y., Zhou, Y., Castiblanco, A., Yang, W., Brown, E. M., and Yang, J. J. (2009) Multiple Ca^{2+}-binding sites in the extracellular domain of the Ca^{2+}-sensing receptor corresponding to cooperative Ca^{2+} response. *Biochemistry* **48**, 388-398

23. Huang, Y., Zhou, Y., Yang, W., Butters, R., Lee, H. W., Li, S., Castiblanco, A., Brown, E. M., and Yang, J. J. (2007) Identification and dissection of Ca^{2+}-binding sites in the extracellular domain of Ca^{2+}-sensing receptor. *J Biol Chem* **282**, 19000-19010

24. Zhang, C., Huang, Y., Jiang, Y., Mulpuri, N., Wei, L., Hamelberg, D., Brown, E. M., and Yang, J. J. (2014) Identification of an L-Phenylalanine Binding Site Enhancing the Cooperative Responses of the Calcium-sensing Receptor to Calcium. *J Biol Chem* **289**, 5296-5309

25. Rey, O., Young, S. H., Yuan, J., Slice, L., and Rozengurt, E. (2005) Amino acid-stimulated Ca^{2+} oscillations produced by the Ca^{2+}-sensing receptor are mediated by a phospholipase C/inositol

1,4,5-trisphosphate-independent pathway that requires G12, Rho, filamin-A, and the actin cytoskeleton. *J Biol Chem* **280**, 22875-22882

26. Young, S. H., and Rozengurt, E. (2002) Amino acids and Ca^{2+} stimulate different patterns of Ca^{2+} oscillations through the Ca^{2+}-sensing receptor. *American journal of physiology. Cell physiology* **282**, C1414-1422

27. Zhang, Z., Qiu, W., Quinn, S. J., Conigrave, A. D., Brown, E. M., and Bai, M. (2002) Three adjacent serines in the extracellular domains of the CaR are required for L-amino acid-mediated potentiation of receptor function. *J Biol Chem* **277**, 33727-33735

28. Jiang, Y., Huang, Y., Wong, H. C., Zhou, Y., Wang, X., Yang, J., Hall, R. A., Brown, E. M., and Yang, J. J. (2010) Elucidation of a novel extracellular calcium-binding site on metabotropic glutamate receptor 1α (mGluR1α) that controls receptor activation. *J Biol Chem* **285**, 33463-33474

29. Reeves, P. J., Callewaert, N., Contreras, R., and Khorana, H. G. (2002) Structure and function in rhodopsin: high-level expression of rhodopsin with restricted and homogeneous N-glycosylation by a tetracycline-inducible N-acetylglucosaminyltransferase I-negative HEK293S stable mammalian cell line. *Proc Natl Acad Sci U S A* **99**, 13419-13424

30. Kornfeld, R., and Kornfeld, S. (1985) Assembly of asparagine-linked oligosaccharides. *Annual review of biochemistry* **54**, 631-664

31. Schachter, H. (1986) Biosynthetic controls that determine the branching and microheterogeneity of protein-bound oligosaccharides. *Biochemistry and cell biology = Biochimie et biologie cellulaire* **64**, 163-181

32. Robertson, M. A., Etchison, J. R., Robertson, J. S., Summers, D. F., and Stanley, P. (1978) Specific changes in the oligosaccharide moieties of VSV grown in different lectin-resistnat CHO cells. *Cell* **13**, 515-526

33. Meng, L., Forouhar, F., Thieker, D., Gao, Z., Ramiah, A., Moniz, H., Xiang, Y., Seetharaman, J., Milaninia, S., Su, M., Bridger, R., Veillon, L., Azadi, P., Kornhaber, G., Wells, L., Montelione, G. T., Woods, R. J., Tong, L., and Moremen, K. W. (2013) Enzymatic basis for N-glycan sialylation: structure of rat alpha2,6-sialyltransferase (ST6GAL1) reveals conserved and unique features for glycan sialylation. *J Biol Chem* **288**, 34680-34698

34. Maniccia, A. W., Yang, W., Li, S. Y., Johnson, J. A., and Yang, J. J. (2006) Using protein design to dissect the effect of charged residues on metal binding and protein stability. *Biochemistry* **45**, 5848-5856

35. Claridge, T. (2009) MNova: NMR data processing, analysis, and prediction software. *J Chem Inf Model* **49**, 1136-1137

36. Delaglio, F., Grzesiek, S., Vuister, G. W., Zhu, G., Pfeifer, J., and Bax, A. (1995) NMRPipe: a multidimensional spectral processing system based on UNIX pipes. *Journal of biomolecular NMR* **6**, 277-293

37. Monleon, D., Colson, K., Moseley, H. N., Anklin, C., Oswald, R., Szyperski, T., and Montelione, G. T. (2002) Rapid analysis of protein backbone resonance assignments using cryogenic probes, a distributed Linux-based computing architecture, and an integrated set of spectral analysis tools. *Journal of structural and functional genomics* **2**, 93-101

38. Huang, Y., Zhou, Y., Wong, H. C., Castiblanco, A., Chen, Y., Brown, E. M., and Yang, J. J. (2010) Calmodulin regulates Ca^{2+}-sensing receptor-mediated Ca^{2+} signaling and its cell surface expression. *J Biol Chem* **285**, 35919-35931

39. Viegas, A., Manso, J., Corvo, M. C., Marques, M. M., and Cabrita, E. J. (2011) Binding of ibuprofen, ketorolac, and diclofenac to COX-1 and COX-2 studied by saturation transfer difference NMR. *Journal of medicinal chemistry* **54**, 8555-8562

40. Tretter, V., Altmann, F., and Marz, L. (1991) Peptide-N4-(N-acetyl-beta-glucosaminyl)asparagine amidase F cannot release glycans with fucose attached alpha 1----3 to the asparagine-linked N-acetylglucosamine residue. *European journal of biochemistry / FEBS* **199**, 647-652

41.   Trimble, R. B., and Tarentino, A. L. (1991) Identification of distinct endoglycosidase (endo) activities in Flavobacterium meningosepticum: endo F1, endo F2, and endo F3. Endo F1 and endo H hydrolyze only high mannose and hybrid glycans. *J Biol Chem* **266**, 1646-1651

42.   Slavik, J. (1982) Anilinonaphthalene sulfonate as a probe of membrane composition and function. *Biochimica et biophysica acta* **694**, 1-25

43.   Schonbrunn, E., Eschenburg, S., Luger, K., Kabsch, W., and Amrhein, N. (2000) Structural basis for the interaction of the fluorescence probe 8-anilino-1-naphthalene sulfonate (ANS) with the antibiotic target MurA. *Proc Natl Acad Sci U S A* **97**, 6345-6349

44.   Streiff, J. H., Juranic, N. O., Macura, S. I., Warner, D. O., Jones, K. A., and Perkins, W. J. (2004) Saturation transfer difference nuclear magnetic resonance spectroscopy as a method for screening proteins for anesthetic binding. *Molecular pharmacology* **66**, 929-935

45.   Bai, M., Trivedi, S., and Brown, E. M. (1998) Dimerization of the extracellular calcium-sensing receptor (CaR) on the cell surface of CaR-transfected HEK293 cells. *J Biol Chem* **273**, 23605-23610

46.   Bai, M. (2004) Structure-function relationship of the extracellular calcium-sensing receptor. *Cell calcium* **35**, 197-207

47.   Kunishima, N., Shimada, Y., Tsuji, Y., Sato, T., Yamamoto, M., Kumasaka, T., Nakanishi, S., Jingami, H., and Morikawa, K. (2000) Structural basis of glutamate recognition by a dimeric metabotropic glutamate receptor. *Nature* **407**, 971-977

48.   Fan, G. F., Ray, K., Zhao, X. M., Goldsmith, P. K., and Spiegel, A. M. (1998) Mutational analysis of the cysteines in the extracellular domain of the human Ca^{2+} receptor: effects on cell surface expression, dimerization and signal transduction. *FEBS letters* **436**, 353-356

49.   Bai, M., Quinn, S., Trivedi, S., Kifor, O., Pearce, S. H., Pollak, M. R., Krapcho, K., Hebert, S. C., and Brown, E. M. (1996) Expression and characterization of inactivating and activating mutations in the human Ca^{2+}_o-sensing receptor. *J Biol Chem* **271**, 19537-19545

50.   Mun, H. C., Culverston, E. L., Franks, A. H., Collyer, C. A., Clifton-Bligh, R. J., and Conigrave, A. D. (2005) A double mutation in the extracellular Ca^{2+}-sensing receptor's venus flytrap domain that selectively disables L-amino acid sensing. *J Biol Chem* **280**, 29067-29072

51.   Rey, O., Young, S. H., Papazyan, R., Shapiro, M. S., and Rozengurt, E. (2006) Requirement of the TRPC1 cation channel in the generation of transient Ca^{2+} oscillations by the calcium-sensing receptor. *J Biol Chem* **281**, 38730-38737

52.   Tsuchiya, D., Kunishima, N., Kamiya, N., Jingami, H., and Morikawa, K. (2002) Structural views of the ligand-binding cores of a metabotropic glutamate receptor complexed with an antagonist and both glutamate and Gd^{3+}. *Proc Natl Acad Sci U S A* **99**, 2660-2665

53.   Muto, T., Tsuchiya, D., Morikawa, K., and Jingami, H. (2007) Structures of the extracellular regions of the group II/III metabotropic glutamate receptors. *Proc Natl Acad Sci U S A* **104**, 3759-3764

FOOTNOTES:

[1]Department of Chemistry, Center for Diagnostics and Therapeutics, Georgia State University; [2]Department of Biochemistry and Molecular Biology and the Complex Carbohydrate Research Center, University of Georgia; [3]Department of Medicine, Division of Endocrinology, Diabetes and Hypertension, Brigham and Women's Hospital, Boston, MA

† These co-authors contributed equally to this work.

§To whom correspondence should be addressed: Jenny J. Yang, Department of Chemistry, Georgia State University, University Plaza, Atlanta, Georgia 30303 USA, Phone : 404-413-5520, Fax: 404-413-5551, email: jenny@gsu.edu

3 The abbreviations used are: CaSR, calcium-sensing receptor; ECD, extracellular domain; STD, Saturation transfer difference; STD-AF, STD amplification factor (STD-AF); GnTI, GlcNAc transferase I; PNGase F, Peptide -N-Glycosidase F; EndoF1, Endoglycosidase F1; ANS, 8-anilino-1-naphthalenesulfonic acid; LRET, luminescence resonance energy transfer; HSQC, heteronuclear single quantum coherence.

Figure legends

Fig. 1 Schematic representation of extracellular domain of the CaSR. (a) The first 26 amino acids are a signal sequence present in the vector. The arrow indicates the beginning of the CaSR ECD sequence. The stop codon is introduced immedaitely after residue 612, resulting in secretion of the receptor into the cell culture medium. Putative glycosylation sites are hightlighted using branches. The loop inserted between D371 and T372 is the engineered Flag-tag. Underlined and labeled regions represent peptide sequences that can be recognized by peptide-specific monoclonal antibody ADD. (b) Schematic figure of protein expression experiment design using 293-F and HEK293S(GnTI⁻) cells. (c) Model structure of CaSR ECD based on the mGluR1 crystal structure (PDB entry: 1ISR) was generated using Swiss-Model. The global view of the ECD is shown in the left panel. Spheres highlighted in red: Ca^{2+}; Green: residues involved in predicted Ca^{2+}-binding sites; Violet: locations of tryptophan residues. L-phenylalanine (in yellow) was positioned at the hinge region between the two lobes by Autodock Vina. Right bottom panel: A zoomed in view of the site 1 Ca^{2+}-binding pocket. Residues involved in Ca^{2+}-binding site 1 are highlighted in green.

Fig. 2 CaSR ECD proteins isolated from cell culture medium are glycosylated
(a) 293-F cells transfected with plasmid encoding 293-F CaSR ECD sequence were continuously cultured for 6 days. Then cell culture medium was collected and underwent the protein purification procedure using nickel affinity column. Representative tracing of A280 measured in milliAU for protein eluted by imidazole. Inset: Coomassie blue staining of the representative fractions from the affinity column separation. The lanes marked "M" are protein molecular weight standards. (b) The same chromatography of protein purification using secreted proteins from HEK293S (GnTI⁻) cells transfected with the CaSR ECD. (c) 293-F CaSR ECD proteins (50 μg) from indicated fractions were heated at 100 ℃ in sample buffer containing β-mercaptoethanol for 5 mins before loading on the gels. (d) GnTI⁻ CaSR ECD proteins were treated using the aforementioned methods in (c). (e) Left two lanes were loaded with 293-F/GnTI⁻ CaSR ECD incubated at room temperature for 5 mins in sample dissociation buffer without reducing reagent; right two lanes were loaded with 293-F/GnTI⁻ CaSR ECD boiled for 5 mins in sample dissociation buffer with β-mercaptoethanol. (f) 293-F CaSR ECD protein (0.5 mg) was incubated with RCA-1 lectin agarose beads overnight at 4℃ followed by a washing step with PBS. Lane 1: Elution fraction using PBS without addition of galactose. Lane 2: Elution fraction using PBS containing 200 mM galactose. Lane 3: 5 μl of the RCA-1 lectin agarose beads after incubation with protein were loaded into the gel as a positive control. The elution fractions were further analyzed by immunoblot using anti-flag antibody. (g) Purified 293-F CaSR ECD (20 μg) was incubated at 100 ℃ for 5 min to denature the protein followed by treatment with PNGase F for 2 hours at 37℃. Protein aliquots with or without PNGase F were loaded in the reducing SDS-Page gel and further analyzed by Western blot using an anti-flag antibody. (h) The purified GnTI⁻CaSR-ECD protein was mixed with Endo F1 at mass ratio 1:3 in 10 mM

16

Tris buffer, pH 7.4 with overnight shaking at 4 ℃. Samples were detected using anti-flag antibody by immunoblot under reducing conditions.

Fig. 3 The secondary structure and stability of purified ECDs. (a) Far-UV CD spectrum of 293-F CaSR ECD in 10 mM Tris, pH 7.2 with or without 2.0 mM Ca^{2+}, at 25 ℃. (b) Far-UV CD spectrum of GnTI- CaSR ECD in 10 mM Tris, pH 7.2 with or without 2.0 mM Ca^{2+}, at 25 ℃. (c) Temperature dependence of the molar ellipticity at 222 nm for 293-F CaSR ECD (closed circle) and GnTI- CaSR ECD (open circle) in 10 mM Tris, pH 7.2. (d) The purified 293-F CaSR ECD protein aliquots were incubated in 10 mM Tris buffer (pH 7.2) at room temperature for the indicated number of days. Samples were then mixed with loading buffer with or without β-mercaptoethanol before being applied in the gel. R: without β-mercaptoethanol. (e) The same experiment as in (d) but with GnTI- CaSR ECD.

Fig. 4 Tryptophan fluorescence titration of CaSR ECDs. The calcium titration was performed in buffer system (10 mM HEPES, 120 mM NaCl and 10 mM KCl, pH 7.2) with a protein concentration of 1.5~2.0 μM. (a) Trp fluorescence spectra of 293-F CaSR ECD in the presence of 0 (---) and 15 mM Ca^{2+} (—). (b) Trp fluorescence spectra of GnTI- CaSR ECD in the presence of 0 (---) or 15 mM Ca^{2+} (—). (c) Calcium titration curve of 293-F CaSR ECD (closed circle: without L-Phe; open circle: in the presence of 10 mM L-Phe). (d) Calcium titration curve of GnTI- CaSR ECD (closed circle: without L-Phe; open circle: in the presence of 10 mM L-Phe).

Fig. 5 Ca^{2+}-induced changes in ANS fluorescence in CaSR ECDs. The ANS assay was performed in a buffer containing 40 μM ANS, 50 mM Tris-HCl and 100 mM KCl (pH 7.4) with either 5 mM EGTA or 3 mM Ca^{2+}. The excitation wavelength was set at 370 nm, and the emission spectra were acquired from 400 to 600 nm. The left panels show ANS fluorescence spectra of CaSR ECD in the presence (—) or the absence of (---) 12 mM Ca^{2+}. The spectrum of ANS alone is shown in gray. The right panels show the calcium titration curve fitted by Hill equation. (a) 293-F CaSR ECD; (b) GnTI- CaSR ECD.

Fig. 6 Tb^{3+} titration curve of CaSR ECDs. Tb^{3+} titration curves of purified CaSR ECDs. The buffer for Tb^{3+} titration consisted of 20 mM PIPES, 135 mM NaCl, and 10 mM KCl (pH 6.8). A pH 6.8 was chosen to prevent formation of $TbOH_3$ during titration. The arrow indicates the increase of the fluorescence. The titration curve was fitted using Hill equation. (a) 293-F CaSR ECD; (b) GnTI- CaSR ECD.

Fig. 7 Tb^{3+} competition assay of CaSR ECDs. Tb^{3+}-Ca^{2+} competition assay of purified CaSR ECDs. The buffer for Tb^{3+} titration consisted of 20 mM PIPES, 135 mM NaCl, and 10 mM KCl (pH 6.8). The arrow indicates the decrease of the fluorescence. (a) 293-F CaSR ECD; (b) GnTI- CaSR ECD.

Fig. 8 Ca^{2+} titration of CaSR ECD monitored by ^1H NMR. ^1H NMR spectra of CaSR ECDs in D_2O and a solution of 10 mM Tris, pH 7.4. Ca^{2+}-induced chemical shift changes in 293-F CaSR ECD were observed at resonances in the main chain amide proton region, such as 7.7 and 7.0 ppm.

Fig. 9 (^1H,^{15}N)-HSQC spectra of 293-F CaSR ECD. The (^1H,^{15}N)-HSQC spectra of CaSR ECDs was obtained in D_2O and a solution of 10 mM Tris, pH 7.4. Left panel: Ca^{2+}-induced chemical shift changes of 293-F CaSR ECD. *Red*: 293-F CaSR ECD without addition of Ca^{2+}; *Orange*, 1 mM Ca^{2+}; Yellow, 3 mM Ca^{2+}; *Green*, 5 mM Ca^{2+}; *Cyan*, 10 mM Ca^{2+}. Middle panel: zoomed in view of each peak. Right panel: the normalized chemical shifts from peak b and c were plotted against calcium concentration and further fitted by the Hill equation.

Fig. 10 Monitoring the ligand-protein interaction via STD NMR. (a) ^1H NMR spectra of a solution of 20 μM GnTI- CaSR ECD in D_2O and 10 mM of Tris (pH 7.8) without (blue line) or with (green line) 1 mM of L-Phe. The difference between spectra at on and off resonance (STD) was shown in red line. The

17

region with the highlighted red box is zoomed in for further analysis in Fig. 10 b, c, and d. (b) Difference between spectra at on and off resonances upon binding of L-Phe at a series of concentrations. The integration of individual peaks was calculated during the L-Phe titration and further used for calculation of the STD amplification factor (STD-AF) in Fig.10 c & d. (c) The average STD-AF from the integrated signal of three major peaks was calculated using equation $STD - AF = \dfrac{I_{ref} - I_{sat}}{I_{ref}} \times \dfrac{[L]_T}{[P]}$ during L-Phe

titration, and was further plotted against increased L-Phe concentration and further fitted using the Hill equation (open circle: without 3.2 mM Ca^{2+}; closed circle: with 3.2 mM Ca^{2+}). (d) Upper panel: The STD signal spectra of 5 mM L-Phe in the presence of 20 μM of GnTI$^-$ CaSR ECD with (Blue) or without 3.2 mM Ca^{2+} (Red). Lower panel: The STD signal spectra of 3 mM L-Asp in the presence of 2.5 mM Ca^{2+} or in the absence of Ca^{2+}.

18

Table 1. Secondary structure of CaSR ECDs at 25 ℃.

	α-Helix		β-Strands		Turns		Unordered	
	Without Ca^{2+}	With Ca^{2+}	Without Ca^{2+}	With Ca^{2+}	Without Ca^{2+}	With Ca^{2+}	Without Ca^{2+}	With Ca^{2+}
293-F ECD	58% ± 1%	55% ± 6%	17% ± 1%	21% ± 4%	6% ± 2%	5% ± 1%	18% ± 4%	15% ± 4%
GnTI⁻ ECD	52% ± 5%	60% ±4%	25% ± 3%	18% ± 1%	5% ± 1%	7% ± 2%	18% ± 3%	18% ± 3%
Modeled ECD	30.0%		17.8%			52.2%		

The signal from CD spectra was further deconvoluted using programs SELCON, CONTIN and CDSSTR. The average numbers of the secondary structure calculations are shown in the table.

Table 2. Summary of dissociation constants and Hill coefficients for CaSR ECDs.

Proteins	Trp Spectrum				ANS Spectrum	
	K_d (mM)	Hill number	K_d (mM) (With 10 mM L-Phe)	Hill number	K_d (mM)	Hill number
293-F ECD	4.9 ± 0.3	1.4 ± 0.1	3.2 ± 0.1*	1.2 ± 0.1	3.8 ± 0.2	2.6 ± 0.2
GnTI⁻ ECD	5.4 ± 0.2	1.6 ± 0.1	3.4 ± 0.3*	1.1 ± 0.1	3.2 ± 0.1	2.3 ± 0.2

*p<0.05

Table 3. Summary of the Tb^{3+} FRET assay.

Proteins	Tb^{3+} Titration		$K_{d,Ca}$ (mM) from Tb^{3+} Competition (μM)	
	K_d (μM)	Hill number	K_d (mM)	Hill number
293-F ECD	36.6 ± 0.4	1.2 ± 0.1	3.7 ± 0.2	1.8 ± 0.1
GnTI⁻ ECD	31.8 ± 0.3	1.3 ± 0.2	2.4 ± 0.2	1.6 ± 0.1

Fig. 1

Fig. 2

22

Fig. 3

Fig. 4

Fig. 5

a 293-F CaSR ECD

b GnTI- CaSR ECD

Fig. 6

a 293-F CaSR ECD

b GnTI- CaSR ECD
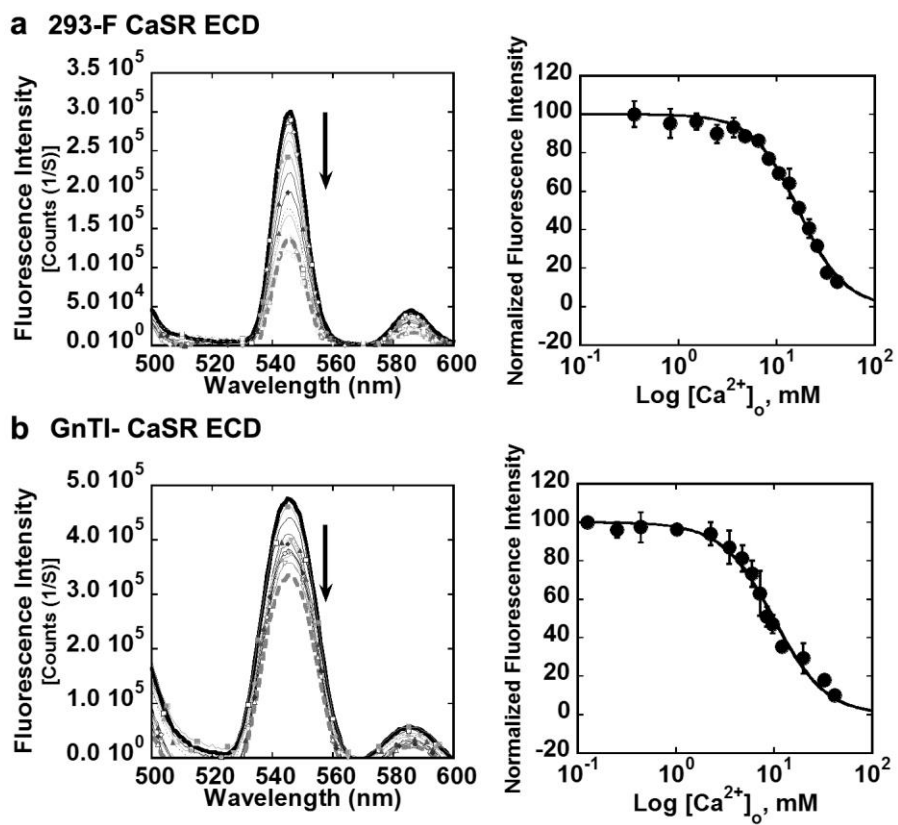
24

Fig. 7

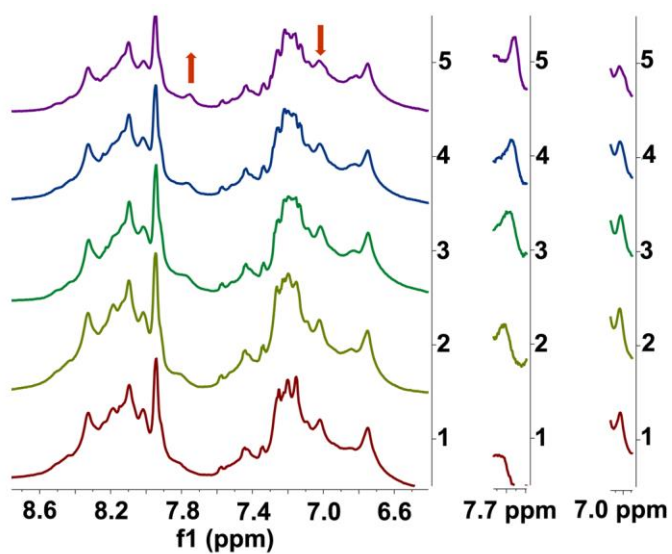a 293-F CaSR ECD
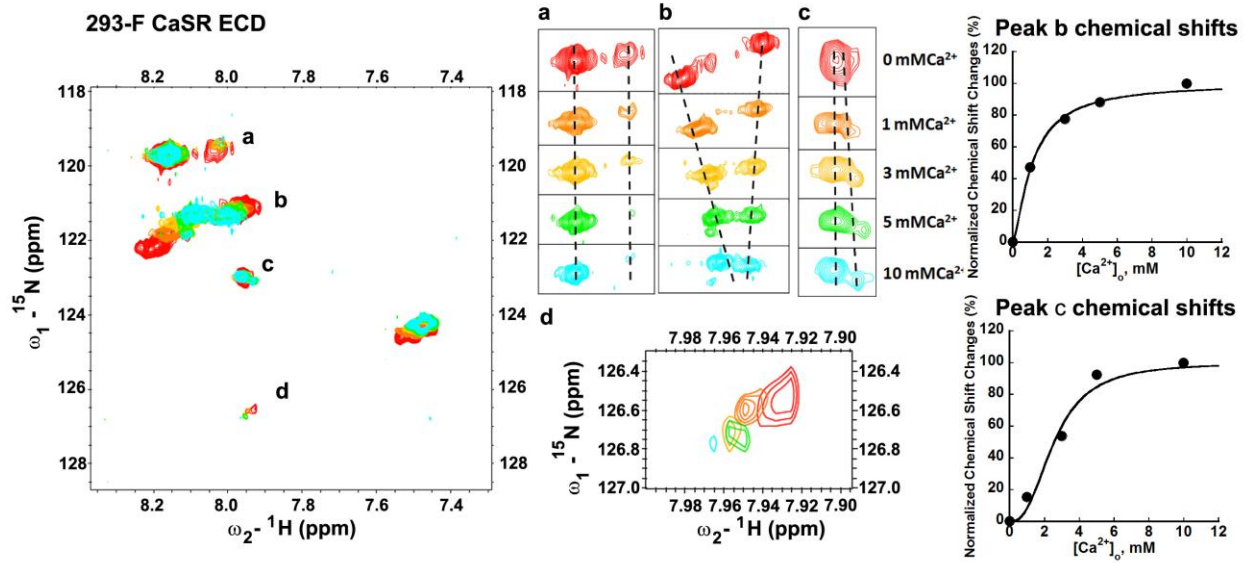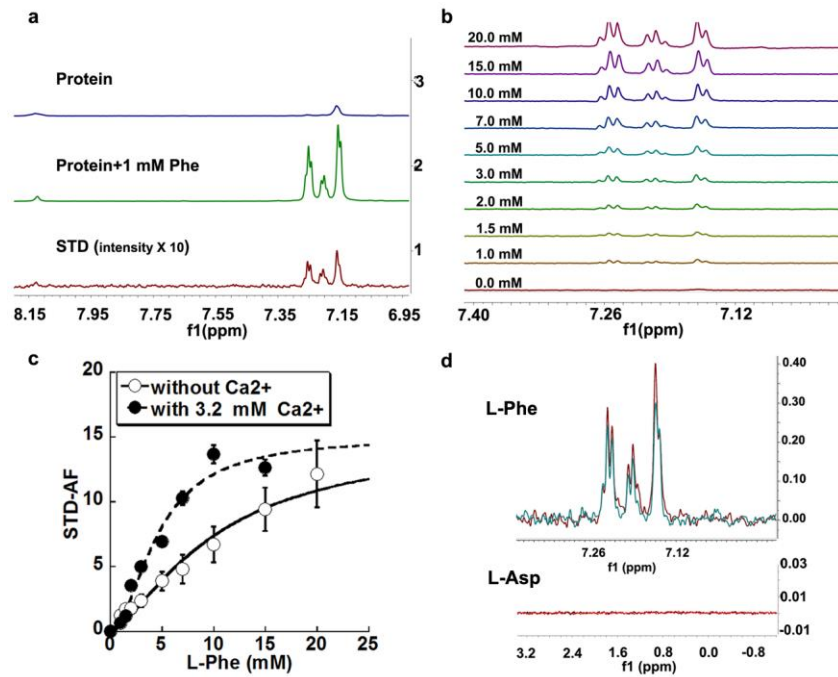
b GnTI- CaSR ECD
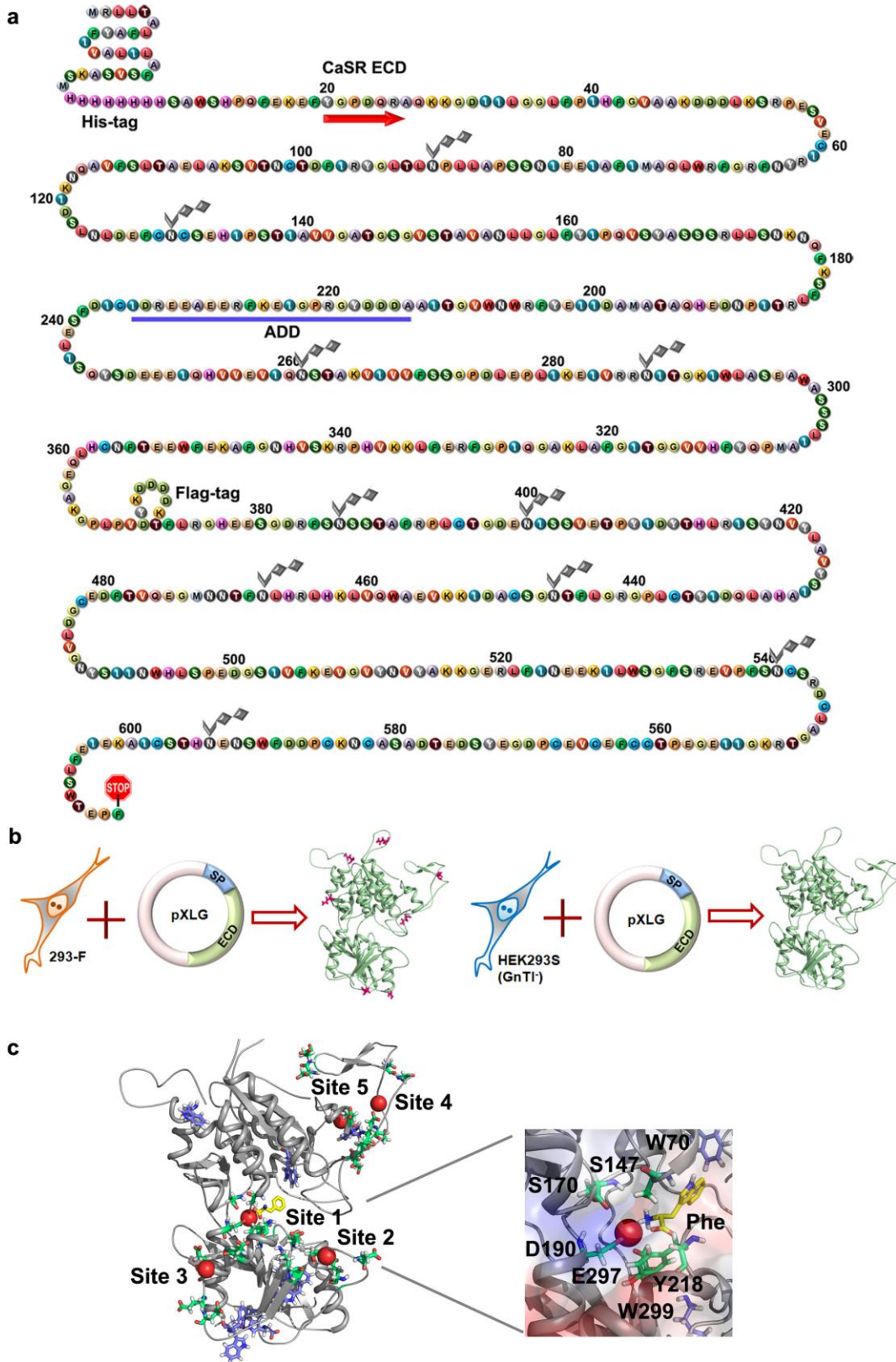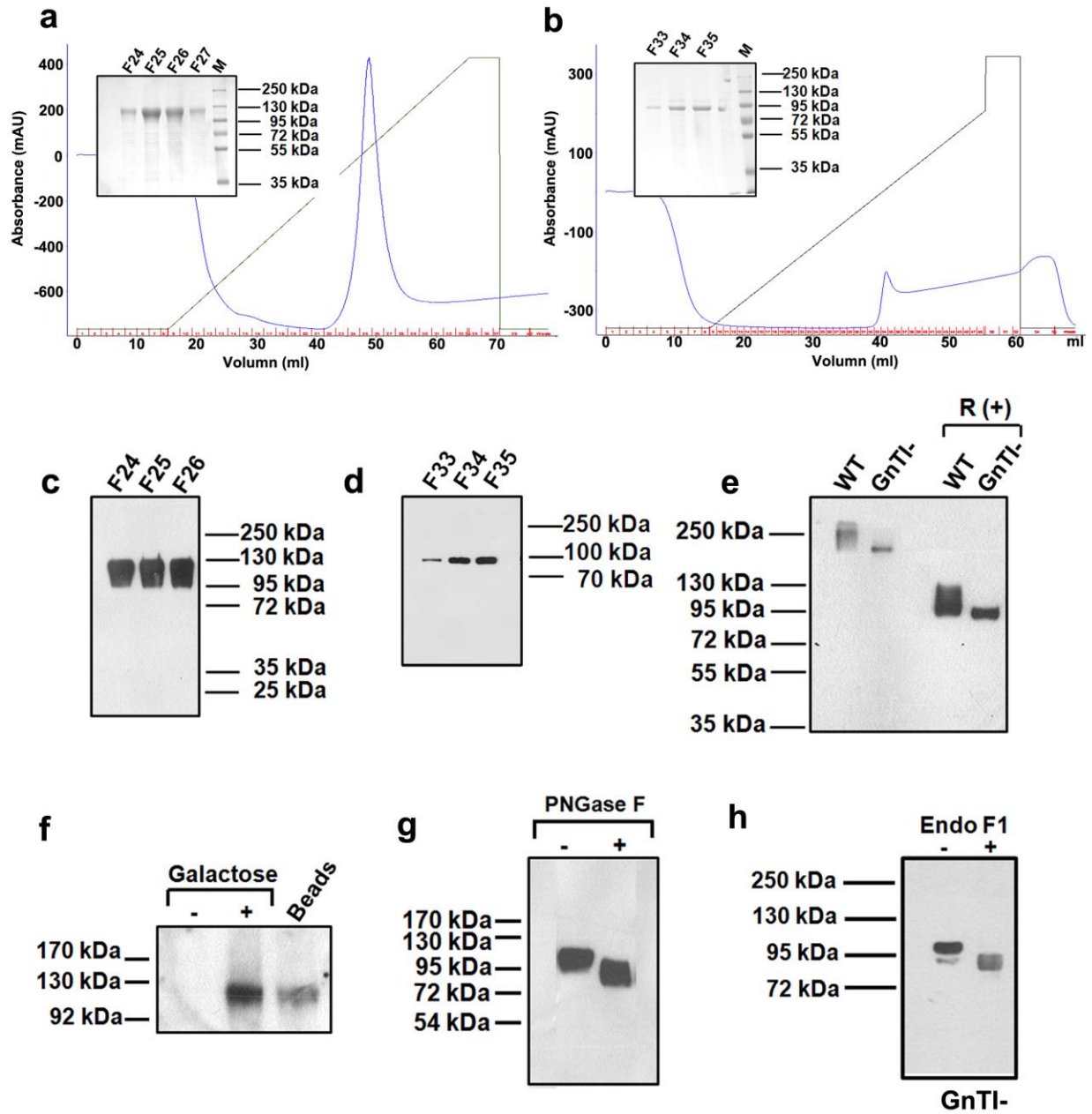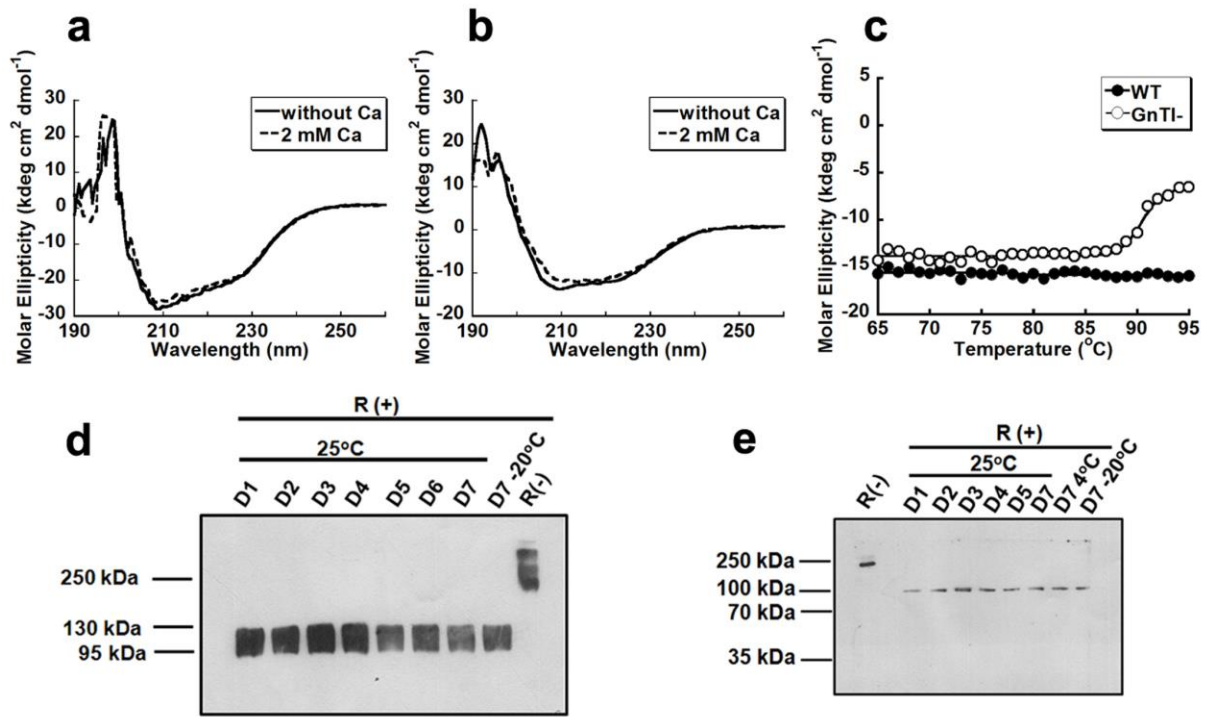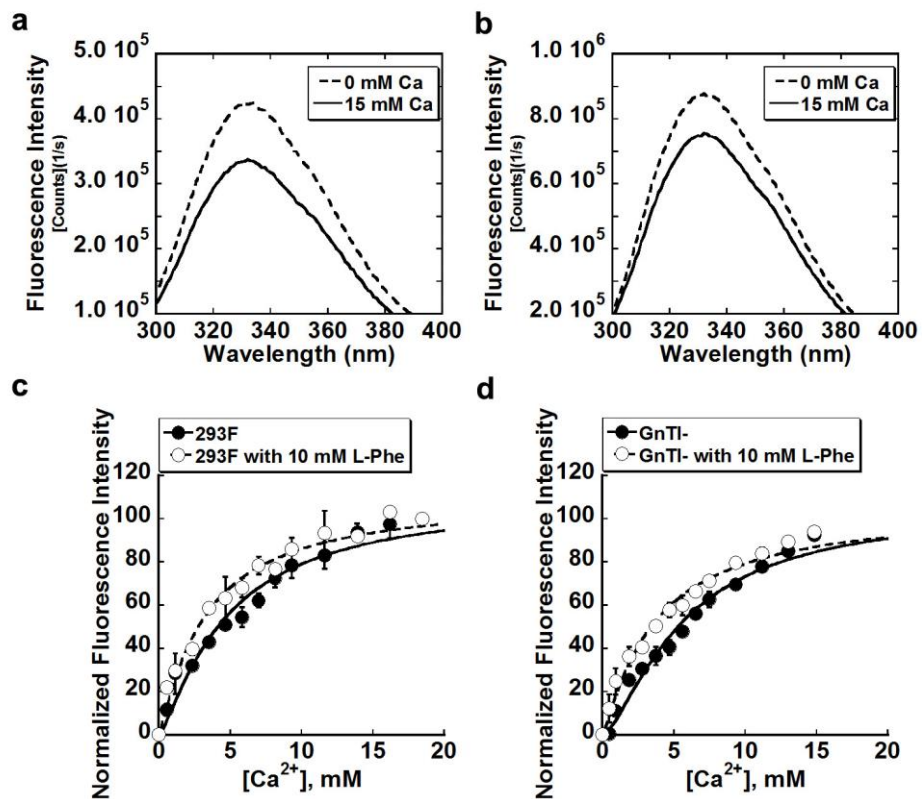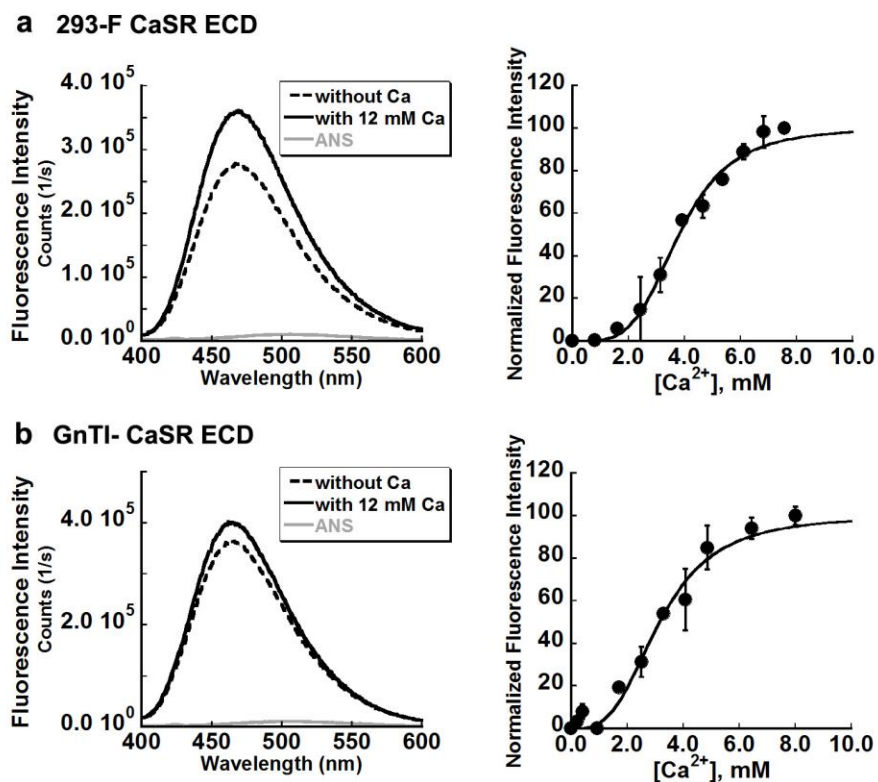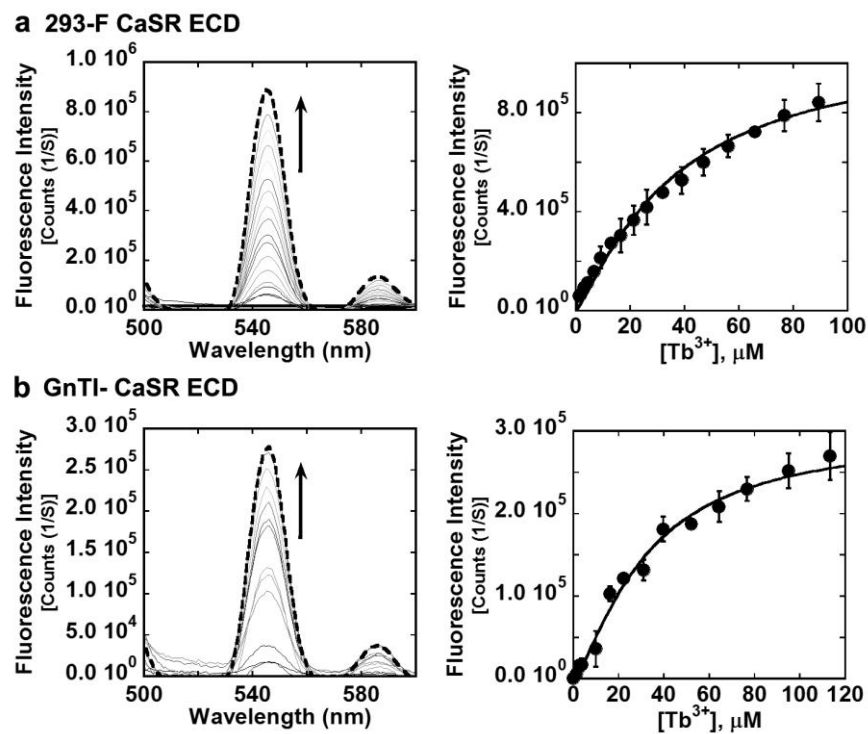
Fig. 8

Fig. 9

Fig. 10

Direct Determination of Multiple Ligand Interactions with the Extracellular Domain of the Calcium Sensing Receptor

Chen Zhang, You Zhuo, Heather A. Moniz, Shuo Wang, Kelley W. Moremen, James H. Prestegard, Edward M. Brown and Jenny J. Yang

Access the most updated version of this article at doi: 10.1074/jbc.M114.604652

Alerts:
- When this article is cited
- When a correction for this article is posted

Click here to choose from all of JBC's e-mail alerts

This article cites 0 references, 0 of which can be accessed free at
http://www.jbc.org/content/early/2014/10/10/jbc.M114.604652.full.html#ref-list-1